available at www.sciencedirect.com

ScienceDirect

journal homepage: www.intl.elsevierhealth.com/journals/dema

In vitro apatite formation on chemically treated (P/M) Ti–13Nb–13Zr

Frank A. Müller[a], *Marco C. Bottino*[b,c,*], *Lenka Müller*[a], *Vinicius A.R. Henriques*[d], *Ulrich Lohbauer*[e], *Ana Helena A. Bressiani*[b], *José C. Bressiani*[b]

[a] *Department of Materials Science (III)-Biomaterials, University of Erlangen-Nuernberg, Erlangen, Germany*
[b] *Materials Science and Technology Center, Institute for Energy and Nuclear Research (IPEN), São Paulo, SP, Brazil*
[c] *Department of Materials Science and Engineering, University of Alabama at Birmingham, 1530 3rd Ave South, BEC 254, Birmingham, AL 35294-4461, United States*
[d] *Materials Division (AMR-IAE) – CTA Brazilian Aerospace Technical Center, São José dos Campos, São Paulo, Brazil*
[e] *Dental Clinic 1 – Operative Dentistry and Periodontology, University of Erlangen-Nuernberg, Erlangen, Germany*

ARTICLE INFO

Article history:
Received 23 March 2006
Received in revised form
16 January 2007
Accepted 5 February 2007

Keywords:
Titanium alloys
Powder metallurgy
Simulated body fluid
Surface modification
Bioactivity

ABSTRACT

Objectives. Titanium alloys are considered the material of choice when used as endosteal part of implants. However, they are not able to bond directly to bone. The objective of this study was to suggest a chemical surface treatment for Ti–13Nb–13Zr to initiate the formation of hydroxy carbonated apatite (HCA) during *in vitro* bioactivity tests in simulated body fluid (SBF).

Methods. Titanium, niobium, and zirconium hydride powders were blended, compacted and sintered. Sintered Ti–13Nb–13Zr samples were etched in HCl, H_3PO_4, and in a mixture of HF + HNO_3, respectively, and subsequently pretreated in NaOH. The influence of acid etching conditions on the microstructure of the Ti–13Nb–13Zr alloys as well as on the rate of HCA formation was evaluated using SEM-EDS, FTIR, and gravimetric analyses.

Results. Sintered Ti–13Nb–13Zr alloys consist of a Widmannstätten ($\alpha + \beta$) microstructure. Exposure of chemically etched and NaOH activated samples to SBF for 1 week leads to the formation of a HCA layer on the surface of HCl as well as H_3PO_4 treated samples. No HCA formation was found on HNO_3 treated samples. After 2 weeks in SBF the mass increase, that can be correlated to the HCA formation rate, was the highest for HCl pretreated samples (2.4 mg/cm^2) followed by H_3PO_4 (0.8 mg/cm^2) and HNO_3 pretreated ones (0.2 mg/cm^2).

Significance. Since the *in vitro* HCA formation from SBF is generally accepted as a typical feature for bioactive materials, it is supposed that HCl etching with subsequent NaOH treatment might enhance the *in vivo* bone-bonding ability of Ti–13Nb–13Zr.

1. Introduction

Metallic biomaterials commonly used in the implantology field are represented by a great variety of alloys which can present different metals as its constituents [1]. Pure titanium and some of its alloys have been extensively used as "load-bearing" implants for biomedical applications, due to their high strength-to-weight ratio, corrosion resistance in the physiological environment, fatigue resistance, and low elastic modulus [2–4].

In its elemental form, titanium has a high melting point (1668 °C) and possesses a hexagonal closely packed (hcp) crys-

* *Corresponding author at*: Department of Materials Science and Engineering, University of Alabama at Birmingham, 1530 3rd Ave South, BEC 254, Birmingham, AL 35294-4461, United States. Tel.: +1 205 934 6970; fax: +1 205 934 8485.
E-mail addresses: mbottino@gmail.com, bottino@uab.edu (M.C. Bottino).
0109-5641/$ – see front matter © 2007 Academy of Dental Materials. Published by Elsevier Ltd. All rights reserved.
doi:10.1016/j.dental.2007.02.005

tal structure α up to a temperature of 883 °C. Above this temperature it transforms into a body centered cubic (bcc) structure β with a lower elastic modulus compared to the α structure [5,6]. Ti-based alloys contain some percentages of α (Al) and β (Nb, V, and Ta) stabilizing elements dissolved in the titanium matrix [6]. Zirconium, which acts both as an α and β isomorphic stabilizer in Ti-based alloys, is also considered to be biologically inert [2–4]. Associated to some investigations which indicated that there is still an unsolved question related to the possible cytotoxic effects of alloying elements such as Al and V [2,3,7,8], it was demonstrated that refractory metals such as niobium, zirconium, and tantalum are considered to be highly biocompatible and also present excellent corrosion resistance [9–12]. Further, some researches described that the biomechanical mismatch between an implant and the surrounding tissue may lead to stress shielding phenomena which may provoke an abnormal stress distribution at the bone–implant interface retarding both bone healing and remodeling [13,14]. Thus, a major goal within the biomedical society is to develop new Ti-based alloys for orthopedic and dental applications with a Young's modulus similar to that of human bone (10–30 GPa). The (α + β) Ti–13Nb–13Zr alloy was formulated at the beginning of the 1990s to be used in orthopedic applications due to its low Young's modulus (40–80 GPa) and its non-toxic composition. It presents tensile values of approximately 1300 MPa and a superior corrosion resistance when compared to Ti–6Al–4V and Ti–6Al–7Nb alloys [9,10,12,15,16].

The powder metallurgy (P/M) technology has proven to be an excellent tool for the near net-shape fabrication of surgical implants due to some inherent advantages, including the capability of precisely adjusting chemical compositions, its feasibility, modulus reduction through the inclusion of pores and also the reduction of costs [1,17–19].

It is well established that the osseointegration process is affected by surface modifications in terms of chemical and physical properties [20]. Two directions – coating technologies and chemical surface treatments – have been reported for titanium and its alloys in order to improve their bone-bonding ability. Among the coating techniques, plasma spraying of hydroxyapatite represents the one most frequently used clinically [21]. However, coating methods are still related to many general problems, including the lack of adherence to the substrate and non-uniformity of the layer thickness [22]. On the other hand, most chemical treatments are focused on obtaining OH-groups on the metal surface that were described to be favorable for enhanced osseointegration [23,24].

The main purpose of this study was to evaluate the influence of different acid etching conditions on the microstructure of (P/M) Ti–13Nb–13Zr surfaces as well as on the rate of hydroxy carbonated apatite (HCA) formation during *in vitro* bioactivity tests in simulated body fluid (SBF).

2. Materials and methods

2.1. *Powder metallurgy*

The starting powders were obtained through a hydrogenation process at elevated temperatures in a vertical furnace for 3 h under a pressure of 10^{-5} Pa [19]. The applied temperature was 500 °C in the case of titanium and 800 °C for niobium and zirconium. After cooling to room temperature, the brittle materials were milled, using a planetary ball mill and a niobium container without argon protecting atmosphere.

The starting elemental powders Ti, Nb and Zr had an average particle size of 31.3, 50.8, and 2.6 μm, respectively. Fig. 1 shows the corresponding SEM micrographs. Calculated powder amounts of 22.2 g Ti, 3.9 g Nb, and 3.9 g Zr were furnace dried for one hour at 100 °C, and blended for 30 min in a planetary mill. Two grams of the blended powder were uniaxially pressed with a pressure of 80 MPa into a square matrix with

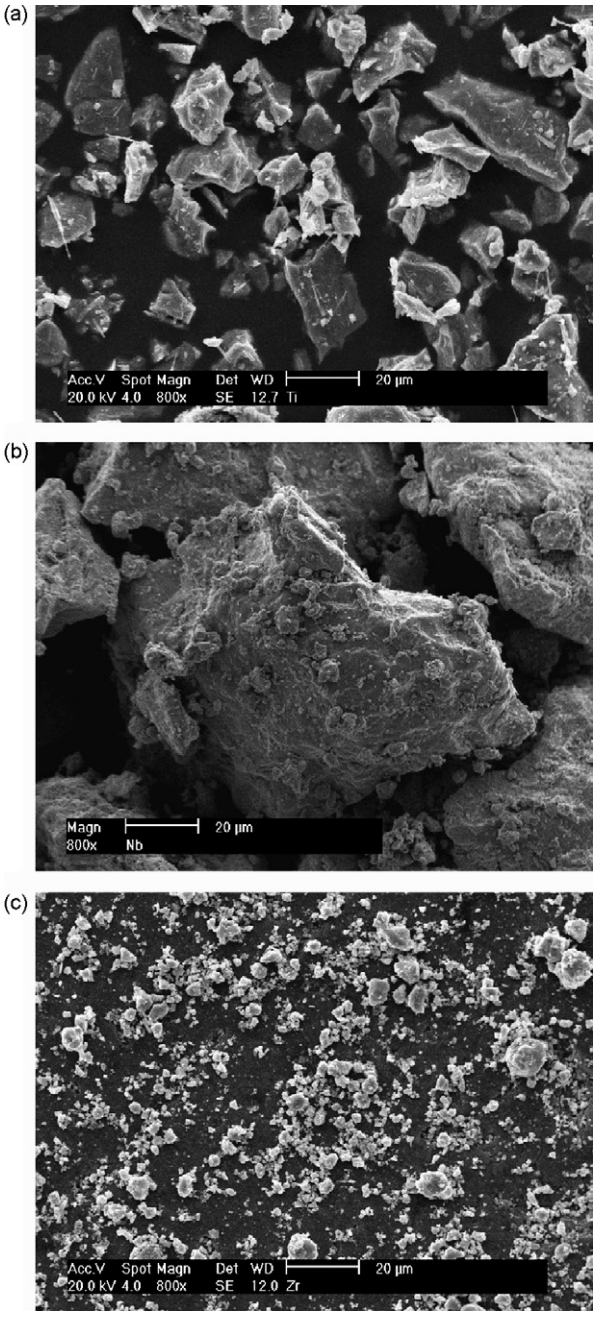

Fig. 1 – SEM micrographs of hydrogenated (a) titanium, (b) niobium, and (c) zirconium powders.

an edge length of 16 mm. Subsequently, the samples were vacuum encapsulated in flexible rubber molds and cold isostatically pressed with a pressure of 300 MPa for 30 s. Green bodies were sintered in a niobium crucible under high vacuum conditions (Thermal Technology Inc., Astro 1000, USA) at 1500 °C for 2 h. The heating rate was 20 °C/min. After sintering the samples were furnace-cooled to room temperature.

2.2. *Chemical surface modification*

Prior to chemical pretreatments the sintered Ti–13Nb–13Zr samples were cut into square plates with an edge length of 10 mm and a thickness of 1 mm and mirror-like polished. Three different etching procedures were performed: (i) samples were etched in 37% HCl under argon atmosphere for 90 min at 50 °C and subsequently for 60 min at 40 °C, (ii) samples were etched in a medium consisting of HF, HNO_3 and H_2O with a ratio of 1:6:18 for 30 s at 20 °C, and (iii) samples were etched in 85% H_3PO_4 for 24 h at 60 °C. Subsequently all specimens were soaked in 10 M NaOH aqueous solution at 60 °C for 24 h, washed with distilled water and dried at 100 °C.

2.3. *Characterization*

The density of the sintered Ti–13Nb–13Zr samples was characterized by measuring the samples' dimensions and weight. X-ray diffraction (XRD) analyses (Cu Kα radiation, $U = 40$ kV, $I = 20$ mA) were performed in order to identify the crystalline phases present in the Ti-based alloys (Rigaku, DMAX 2000, Japan). Data were collected in the range of $2\theta = 25$–$80°$ with a step size of 0.02° and a scan speed of 0.15 °/min. Metallographic preparation was carried out according to conventional techniques. The microstructure was revealed by swabbing the samples with a Kroll solution (3 ml HF:6 ml HNO_3:100 ml H_2O) for 10–20 s [25].

The average surface roughness R_a of untreated as well as chemically activated samples (number of samples for each treatment $n = 3$; evaluation length = 150 μm) was measured by confocal laser scanning microscopy (CLSM) (Leica, TCS SL, Germany). The activated samples were exposed to SBF with ionic concentrations nearly equal to human blood plasma. The SBF solution with an HCO_3^- concentration of 10 mmol/l was prepared by mixing concentrated solutions of KCl, NaCl $NaHCO_3$, $MgSO_4 \cdot 7H_2O$, $CaCl_2$ and KH_2PO_4 into double distilled water and buffered with tris-hydroxymethyl aminomethan and HCl to pH 7.4 at 37 °C, according to a procedure described in [26]. Sodium azide (NaN_3) was added to the solution to inhibit the growth of bacteria.

The microstructure of the precipitated HCA layer was characterized by scanning electron microscopy (SEM) (FEI, Quanta 200, The Netherlands) on gold coated samples. Energy dispersive spectroscopy (EDS) (Oxford Instruments, Inca x-sight, UK) was used to quantify the amount of Na in the surface of pretreated samples ($n = 3$, spot size = 1 μm^2). Sample–solution interactions were quantified after 2 weeks in SBF on the basis of gravimetric analyses ($n = 3$) by using an analytical balance (Ohaus, AP210, USA). Fourier-transform infrared (FTIR) spectra were measured in transmission using the KBr-technique in the range from 4000 to 400 cm^{-1} at a resolution of 4 cm^{-1} (Nicolet Instruments, Impact 420, USA). Approximately 1 mg of the HCA coating was removed from the substrate, mixed with 300 mg of dry KBr powder and ground using an agate mortar and pestle.

3. Results

After sintering at 1500 °C for 2 h, the Ti–13Nb–13Zr samples were densified to a final density of 4.66 g/cm^3, representing 93% of the theoretical one. Fig. 2a shows an SEM micrograph of the Ti–13Nb–13Zr microstructure with residual closed pores, which are characteristic for the final stage of sintering. Fig. 2b shows the same microstructure at a higher resolution, where the formation of the classical Widmannstätten biphasic (α + β) structure, that is characterized by groups of parallel α-plates embedded into a β-matrix, can be observed. XRD analysis also revealed the α as well as the β phase to be present in the sintered Ti–13Nb–13Zr alloy (Fig. 3).

Fig. 4 shows the Ti–13Nb–13Zr surface after different acid etchings and after subsequent NaOH activation, respectively. The average surface roughness of HCl treated (Fig. 4a, $R_a = 844 \pm 6$ nm), H_3PO_4 treated (Fig. 4e, $R_a = 1437 \pm 99$ nm) as well as HF:HNO_3:H_2O treated samples (Fig. 4c, $R_a = 865 \pm 23$ nm) significantly ($p < 0.05$) exceeds that of untreated samples ($R_a = 501 \pm 52$ nm). During subsequent activation in

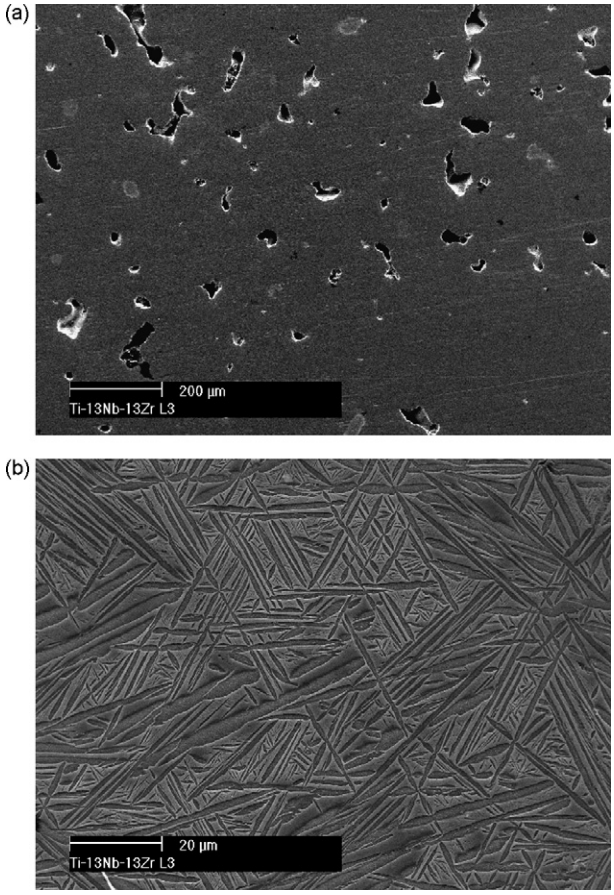

Fig. 2 – SEM photomicrographs of the Ti–13Nb–13Zr alloy sintered at 1500 °C: (a) general view with residual pores and (b) Widmannstätten-like microstructure.

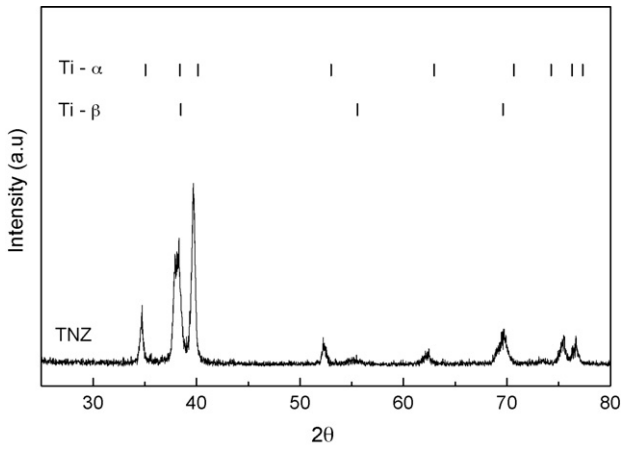

Fig. 3 – XRD patterns of the Ti–13Nb–13Zr alloy after sintering at 1500 °C for 2 h.

NaOH the surface microroughness remains unchanged for all samples. However, microcracks were in particular found on the surface of H_3PO_4 (Fig. 4d) and HF:HNO_3:H_2O (Fig. 4f) pretreated samples, whereas no cracks are visible in HCl (Fig. 4b) pretreated samples. The quantity of Na^+ incorporated into the materials surface after NaOH activation was comparable for different acid etching procedures and amounts to 4.11 ± 0.11 at.% for HCl treated, 4.80 ± 0.15 at.% for H_3PO_4 treated and 3.98 ± 0.09 at.% for HNO_3 treated samples. According to earlier results obtained for commercially pure titanium a hydrated sodium titanate gel-like layer is formed at the sample surface [24,27].

Fig. 5 shows SEM micrographs of acid etched and NaOH treated Ti–13Nb–13Zr surfaces after exposure to SBF for one and 2 weeks, respectively. HCl- as well as H_3PO_4-etching in combination with the NaOH treatment leads to the formation of HCA agglomerates after 1 week in SBF (Fig. 5a and e). Fig. 6 shows FTIR spectra of the HCA layers deposited on pretreated Ti–13Nb–13Zr surfaces. A broad absorption band

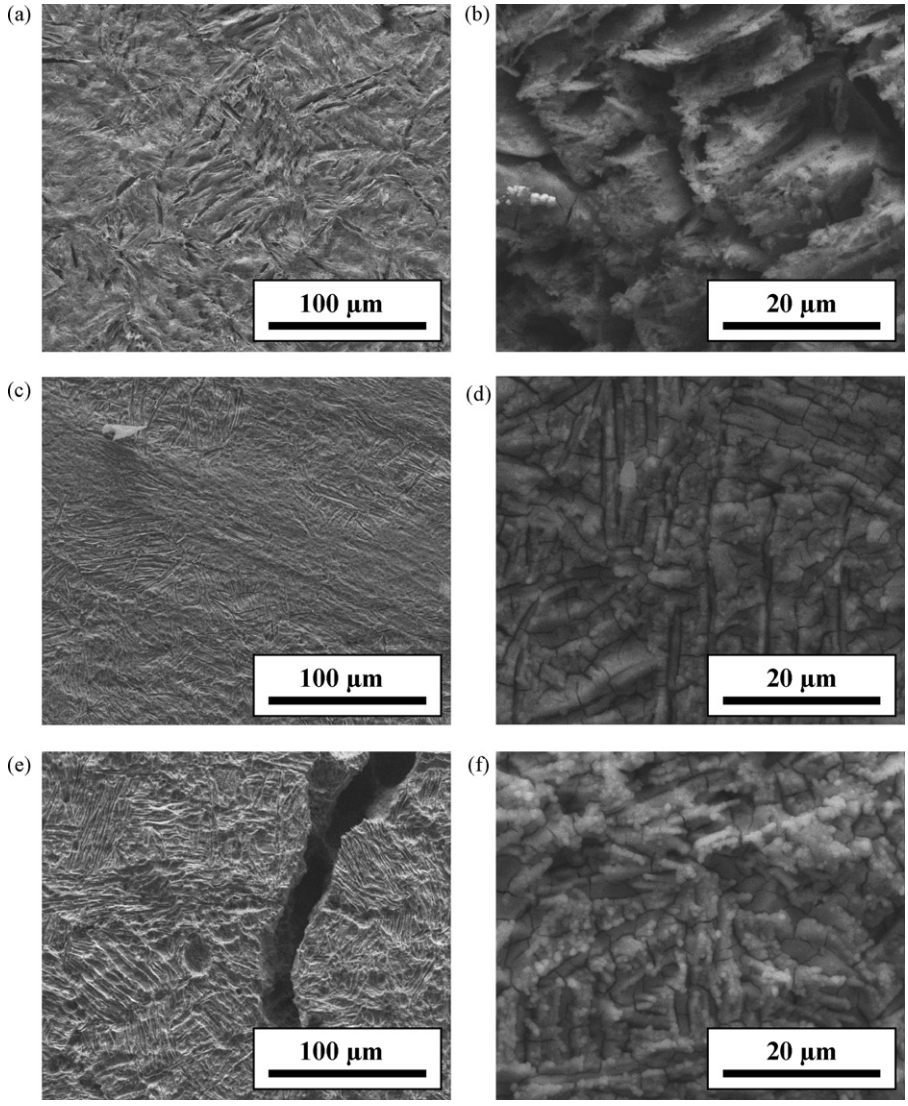

Fig. 4 – SEM micrographs of (a) HCl etched surface, (b) subsequently activated with NaOH; (c) HF:HNO_3:H_2O etched surface, (d) subsequently activated with NaOH; and (e) H_3PO_4 etched surface, (f) subsequently activated with NaOH.

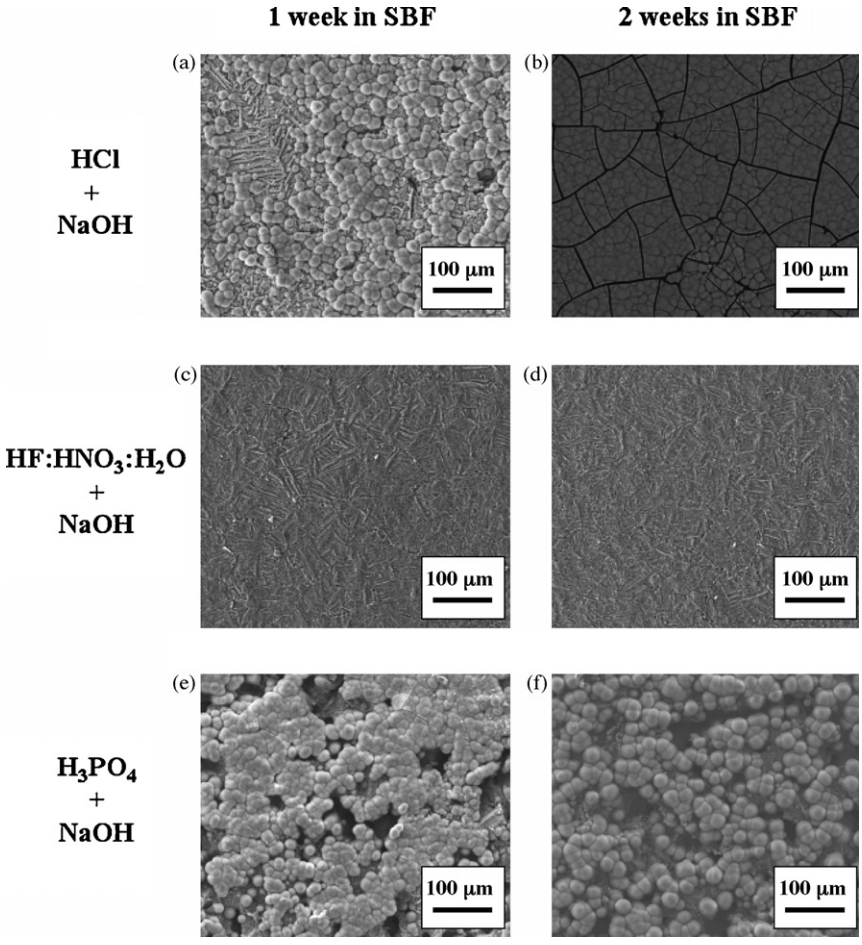

Fig. 5 – SEM micrographs of pretreated Ti–13Nb–13Zr surfaces after exposure to SBF.

at 3450 cm^{-1} and the bending mode at 1650 cm^{-1} proved the presence of H_2O in the biomimetic apatite coatings. The asymmetric P–O stretching mode (ν_3) of the P–O bond of the PO_4^{3-} group (1200–960 cm^{-1}) indicated a deformation of the phosphate coordination symmetry from their tetrahedral structure. The triple (ν_4) and double (ν_2) degenerated bending modes of the O–P–O bonds were found at 604, 567 and 474 cm^{-1}. A characteristic peak at 875 cm^{-1} indicates the presence of HPO_4^{2-} in the crystal lattice. The bands at 1500, 1430 and 875 cm^{-1} were assigned to the CO_3^{2-} group of B-type carbonated apatite with the general formula $Ca_{10-x}(HPO_4)_{x-y}(CO_3)_y(PO_4)_{6-x}(OH)_{2-x}$ [26]. However, the bands at 1490, 1070 and 875 cm^{-1} found in HCl pretreated samples (Fig. 6a) can also be associated with amorphous calcium carbonate. In H_3PO_4 pretreated samples these bands cannot be observed (Fig. 6b).

The mass increase related to the geometric surface area after 2 weeks in SBF was the highest for HCl pretreated samples (2.44 ± 0.18 mg/cm^2) followed by H_3PO_4 (0.80 ± 0.24 mg/cm^2) and HNO_3 pretreated ones (0.21 ± 0.07 mg/cm^2). The HCl-treated surface was completely covered with HCA layer within 2 weeks in SBF (visible cracks result from drying) (Fig. 5b). In contrast, the amount of HCA that was formed on the H_3PO_4 pretreated surface was not increased after 2 weeks of exposure compared to samples that were exposed for only 1 week (Fig. 5f). For HNO_3 pretreated samples HCA formation could only be observed on single sites not homogeneously distributed over the samples surface (Fig. 5c and d).

4. Discussion

When exposed to SBF, alkali ions are released from the gel-like sodium titanate layer that covers the Ti–13Nb–13Zr surface after NaOH treatment. As a consequence hydronium ions enter into the surface layer, resulting in the formation of Ti–OH groups in the surface. The released Na^+ ions increase the degree of supersaturation of the soaking solution with respect to apatite by increasing pH, and Ti–OH groups induce apatite nucleation on the titanium surface by an incorporation of Ca^{2+} followed by a reaction with PO_4^{3-} [24].

Differences in the rate of HCA formation on differently etched Ti–13Nb–13Zr surfaces might be explained by differences in the surface composition depending on the etching conditions. Titanium and its alloys develop very stable surface oxides with high integrity, tenacity and good adherence. The composition of this passive oxide film was shown to be composed of an amorphous TiO_2 outer layer with 10–20 nm

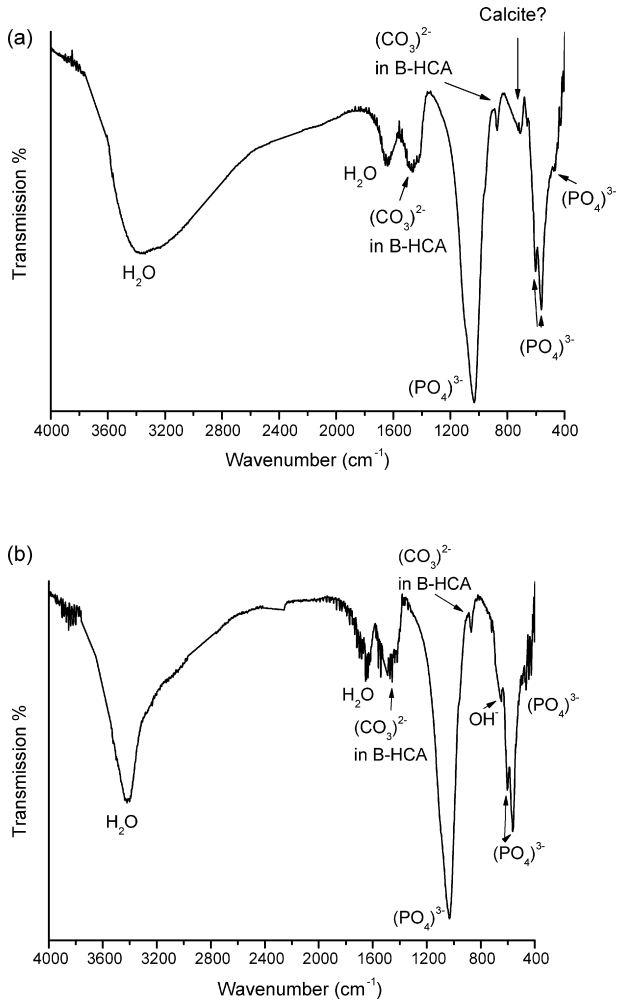

Fig. 6 – FTIR spectra of HCA precipitates deposited on (a) HCl + NaOH and (b) H_3PO_4 + NaOH pretreated Ti–13Nb–13Zr surfaces.

thickness and an intermediate TiO_x layer with 10–40 nm thickness, in contact with the metallic substrate [28]. The corrosion resistance of titanium alloys is limited in strong, highly reducing acid media, such as moderately or highly concentrated solutions of HCl and H_3PO_4 at all concentrations. Corrosion rates increase with increasing acid concentration and temperature.

The passive oxide film dissolves in HCl under inert atmosphere and restores itself in the presence of air or water. Since it was not exposed to high temperature, it can be supposed that this titanium oxide layer is thinner than the initial one. According to earlier results obtained for commercially pure titanium [24], sodium titanate can form after subsequent alkali treatment and react with Ca^{2+} from the solution to form a calcium titanate during the initial phase of exposure to SBF. Subsequently PO_4^{3-} is attracted and the nucleation and subsequent growth of apatite starts.

In H_3PO_4, anodizing of the surface takes place, which strengthens and densifies the existing thin passive layers, resulting in a spectrum of surface colors depending on the passive film thickness. The further leaching of titanium in NaOH seems to be insufficient to completely dissolve the passive oxide layer and to form sodium titanate. However, previous works showed that phosphate ions can be incorporated into the anodic layer on titanium and Ti–6Al–4V and in turn enhance apatite formation [29,30]. The insufficient formation of HCA in the surface of H_3PO_4 and NaOH treated Ti–13Nb–13Zr seems to be the result of a competition between the positive effect of phosphate ion incorporation and the negative effect of passive film densification.

In the case of HNO_3 pretreated Ti–13Nb–13Zr samples the rate of HCA formation was significantly reduced compared to HCl and H_3PO_4 treated samples, respectively. Titanium is highly resistant to oxidizing acids (e.g. HNO_3) over a wide range of concentrations and temperatures, assuring oxide film stability and densification. As a consequence of the corrosion resistance of the passivated layer to alkali media, no sodium titanate layer can be formed on the samples surface during activation with NaOH, and consequently, no apatite formation was observed.

5. Conclusion

A combination of acid etching and subsequent NaOH treatment was successfully used to initiate *in vitro* HCA formation on the surface of (P/M) Ti–13Nb–13Zr alloys. The rate of HCA formation was the highest for samples etched in HCl.

Acknowledgments

This investigation was supported by grants (# 03/10049-5 and 03/06697-1) from the Fundação de Amparo à Pesquisa do Estado de São Paulo (FAPESP, Brazil). Financial support of the Deutsche Forschungsgemeinschaft (MU1803/1) and CAPES/DAAD (PROBRAL 138) is gratefully acknowledged. The authors are thankful to DEMAR/FAENQUIL for niobium supply.

REFERENCES

[1] Pypen CMJM, Dessein K, Helsen JA, Gomes M, Leenders H, Bruijn JD. Comparison of the cytotoxicity of molybdenum as powder and as alloying element in a niobium-molybdenum alloy. J Mater Sci-Mater Med 1998;9:761–5.
[2] Okazaki Y, Nishimura E, Nakada E, Kobayashi K. Surface analysis of Ti–15Zr–4Nb–4Ta alloy after implantation in rat tibia. Biomaterials 2001;22:599–607.
[3] Okazaki Y, Rao S, Ito Y, Tateishi T. Corrosion resistance, mechanical properties and cytocompatibility of new Ti alloys without Al and V. Biomaterials 1998;19:1197–215.
[4] Eisenbarth E, Velten D, Müller M, Thull R, Breme. Biocompatibility of β-stabilizing elements of titanium alloys. Biomaterials 2004;25:5705–13.
[5] Collings EW. The physical metallurgy of titanium alloys. In: Gegel HL, editor. ASM series in metal processing. Cleveland, Metals Park, OH: Edward Arnold Publications; 1984.
[6] Liu X, Chu PK, Ding C. Surface modification of titanium, titanium alloys, and related materials for biomedical applications. Mater Sci Eng R 2004;47:49–121.
[7] Kuroda D, Niinomi M, Morinaga M, Kato Y, Yashiro T. Design and mechanical properties of new β type titanium alloys for implant materials. Mater Sci Eng A 1998;243(1–2):244–9.

[8] Berthon G. Aluminium speciation in relation to aluminium bioavailability, metabolism and toxicity. Coord Chem Rev 2002;228:319–41.
[9] Davidson JA, Mishra AK, Kovacs P, Poggie RA. New surface hardened, low-modulus, corrosion-resistant Ti–13Nb–13Zr alloy for total hip arthroplasty. Bio-Med Mater Eng 1994;4:231–43.
[10] Yu SY, Scully JR. Corrosion and passivity of Ti–13% Nb–13% Zr in comparison to other biomedical implant alloys. Corrosion 1997;53:965–76.
[11] Matsuno H, Yokohama A, Watari F, Uo M, Kawasaki T. Biocompatibility and osteogenesis of refractory metal implants, titanium, hafnium, niobium, tantalum and rhenium. Biomaterials 2001;22:1253–62.
[12] Geetha M, Mudali UK, Gogia AK, Asokamani R, Raj B. Influence of microstructure and alloying elements on corrosion behavior of Ti–13Nb–13Zr alloy. Corros Sci 2004;46:877–92.
[13] Moyen BJ, Lahey Jr PJ, Weinberg EH, Harris WH. Effects on intact femora of dogs of the application and removal of metal plates. A metabolic and structural study comparing stiffer and more flexible plates. J Bone Joint Surg Am 1978;60:940–7.
[14] Oh IK, Nomura N, Hanada S. Mechanical properties of porous titanium compacts prepared by powder sintering. Scripta Mater 2003;49:1197–202.
[15] Wang K. The use of titanium for medical applications in the USA. Mater Sci Eng A 1996;213:134–7.
[16] Semiatin SL, Seetharaman V, Weiss I. The thermomechanical processing of alpha/beta titanium alloys. JOM-J Min Met Mater S 1997;49:33–9.
[17] Henriques VAR, Bellinati CE, Silva CRM. Production of Ti–6% Al–7% Nb alloy by powder metallurgy (P/M). J Mater Process Technol 2001;118:212–5.
[18] Wojnar L, Dabrowski JR, Oksiuta Z. Porosity structure and mechanical properties of vitalium-type alloy for implants. Mater Charact 2001;46:221–5.
[19] Taddei EB, Henriques VAR, Silva CRM, Cairo CAA. Production of new titanium alloy for orthopedic implants. Mater Sci Eng C 2004;24:683–7.
[20] Lemons JE. Biomaterials, biomechanics, tissue healing, and immediate-function dental implants. J Oral Implantol 2004;30:318–24.
[21] Ducheyne P, van Raemdonck W, Heughbaert JC, Heughbaert M. Structural analysis of hydroxyapatite coatings on titanium. Biomaterials 1986;7:97–103.
[22] Thomas KA, Kay JF, Cook SD, Jarcho M. The effect of surface macrotexture and hydroxylapatite coating on the mechanical strengths and histologic profiles of titanium implant materials. J Biomed Mater Res 1987;21: 1395–406.
[23] Kokubo T, Miyaji F, Kim HM, Nakamura T. Spontaneous formation of bonelike apatite layer on chemically treated titanium metals. J Am Ceram Soc 1996;79:1127–9.
[24] Jonásová L, Müller FA, Helebrant A, Strnad J, Greil P. Biomimetic apatite formation on chemically treated titanium. Biomaterials 2004;25:1187–94.
[25] Boyer RR. Aerospace applications of beta titanium alloys. JOM-J Min Met Mater S 1994;46:20–3.
[26] Müller L, Müller FA. Preparation of SBF with different HCO_3^- content and its influence on the composition of biomimetic apatites. Acta Biomater 2006;2:181–9.
[27] Kokubo T, Kim HM, Kawashita M, Nakamura T. Bioactive metals: preparation and properties. J Mater Sci-Mater Med 2004;15:99–107.
[28] Pouilleau J, Devilliers D, Garrido F, Durand-Vidal S, Mahé E. Structure and composition of passive titanium oxide films. Mater Sci Eng B 1997;47:235–43.
[29] Krasicka-Cydzik E. Gel-like layer development during formation of thin anodic films on titanium in phosphoric acid solution. Corros Sci 2004;46:2487–502.
[30] Hanawa T, Mamoru O. Calcium phosphate naturally formed on titanium in electrolyte solution. Biomaterials 1991;12:767–74.